Ionics (2015) 21:1843–1849
DOI 10.1007/s11581-015-1374-6

ORIGINAL PAPER

Preparation and electrochemical performance of spinel $LiNi_{0.5-x}Mn_{1.5+x}O_4$ (x=0, 0.05, 0.1) hollow microspheres as cathode materials for lithium-ion batteries

W. W. Wu · J. J. Chen · S. Cheng · H. F. Xiang

Received: 7 December 2014 / Revised: 5 January 2015 / Accepted: 13 January 2015 / Published online: 29 January 2015

Abstract The spinel $LiNi_{0.5-x}Mn_{1.5+x}O_4$ (x=0, 0.05, 0.1) including $LiNi_{0.5}Mn_{1.5}O_4$, $LiNi_{0.45}Mn_{1.55}O_4$, and $LiNi_{0.4}Mn_{1.6}O_4$ hollow microspheres has been prepared by adjusting the stoichiometric ratios of Ni and Mn with an impregnation method followed by a simple solid-state reaction. They are characterized by X-ray diffraction, Fourier transform infrared spectroscopy, scanning electron microscope, high-resolution transmission electron microscope, X-ray photoelectron spectroscopy, and electrochemical tests. The results show that $LiNi_{0.5}Mn_{1.5}O_4$ is the ordered with the space group of $P4_332$, but $LiNi_{0.45}Mn_{1.55}O_4$ and $LiNi_{0.4}Mn_{1.6}O_4$ are the disordered with the space group of Fd3m. All the three types of hollow microspheres have the similar primary particles. Compared to $LiNi_{0.5}Mn_{1.5}O_4$, partial Ni atoms are substituted by Mn atoms in $LiNi_{0.45}Mn_{1.55}O_4$ and $LiNi_{0.4}Mn_{1.6}O_4$ lattices along with incorporation of small amounts of Mn^{3+}. Although the ordered $LiNi_{0.5}Mn_{1.5}O_4$ hollow microspheres deliver the highest capacity of 128.5 mAh/g at 1 C among the three types of spinel materials, the disordered $LiNi_{0.45}Mn_{1.55}O_4$ hollow microspheres exhibit the highest capacity of 96.8 mAh/g at 10 C. The superior rate capability of $LiNi_{0.45}Mn_{1.55}O_4$ hollow microspheres is attributed to the combination of the increased electronic conductivity and Li^+-ion diffusion by moderate Mn^{3+} incorporation, along with the hierarchical structure.

Keywords Lithium nickel manganese oxide · Hollow microspheres · Disordered · Ordered · Lithium-ion batteries

W. W. Wu · J. J. Chen · S. Cheng · H. F. Xiang (✉)
School of Materials Science & Engineering, Hefei University of Technology, Hefei, Anhui 230009, China
e-mail: hfxiang@hfut.edu.cn

Introduction

Lithium-ion batteries (LIBs) have been widely used in consumer electronics products, owing to their highest energy density among the present commercial rechargeable batteries [1, 2]. However, for the applications in electric vehicles and smart grids, it is desired to further increase their energy density. Since energy of a battery is the product of stored capacity and output voltage, the approaches to increase energy density include increasing the voltage of cathode materials and the capacity of electrode materials. Spinel $LiNi_{0.5}Mn_{1.5}O_4$ as the representative of high-voltage cathode can provide a working plateau at 4.7 V and thus offer much higher energy density (650 Wh/kg) than those commercial 3.2 or 4 V class cathode materials, such as $LiCoO_2$ (540 Wh/kg), $LiMn_2O_4$ (500 Wh/kg), and $LiFePO_4$ (500 Wh/kg) [3]. Therefore, high-voltage $LiNi_{0.5}Mn_{1.5}O_4$ has been regarded as one of the most promising cathode materials for high-energy LIBs [4].

Spinel $LiNi_{0.5}Mn_{1.5}O_4$ has two types of space groups: $P4_332$ and Fd3m [5]. The former has Ni and Mn orderly distributed in the 4a and 12d octahedral sites, respectively; thus, this $P4_332$-type spinel is called ordered $LiNi_{0.5}Mn_{1.5}O_4$. On the contrary, because of random Ni/Mn occupation in the 16d octahedral sites, the Fd3m-type spinel is named disordered $LiNi_{0.5}Mn_{1.5}O_4$. Usually, the disordered $LiNi_{0.5}Mn_{1.5}O_4$ is facile to be received during high-temperature (above 700 °C) preparation, along with a small amount of oxygen loss, as $LiNi_{0.5}Mn_{1.5}O_{4-\delta}$. The significant difference between the ordered and the disordered is the presence of Mn^{3+} in the latter, which leads to their obviously different electrochemical properties. Mn^{3+} can disproportionate to Mn^{4+} and Mn^{2+}, which has the high solubility in the electrolyte. Therefore, the disordered $LiNi_{0.5}Mn_{1.5}O_{4-\delta}$ has the inferior cycling stability than ordered $LiNi_{0.5}Mn_{1.5}O_4$ [4–6]. However, Mn^{3+} in the disordered phase has the positive contribution on charge

transfer because of its higher electronic conductivity and bigger ionic radius than Mn^{4+}. Many literatures reported that disordered Fd3m-type $LiNi_{0.5}Mn_{1.5}O_{4-\delta}$ has better rate capability than ordered $P4_332$-type $LiNi_{0.5}Mn_{1.5}O_4$ [5, 7–11]. What is confusing is that Mn^{3+} only exists at a small regime of the electrochemical reaction (beginning of charging and end of discharging), and its contribution on electronic conductivity should be very limited [12].

Recently, we synthesized hierarchically nanostructured framework ordered $LiNi_{0.5}Mn_{1.5}O_4$ hollow microspheres which exhibited superior rate capability than the disordered $LiNi_{0.5}Mn_{1.5}O_4$ hollow microspheres. And we found that the better rate capability can be attributed to the signal-crystal structure on the surface of the ordered $LiNi_{0.5}Mn_{1.5}O_4$, which is helpful for the fast Li^+-ion insertion/extraction kinetics [13]. In that work, we introduced Mn^{3+} and prepared the disordered $LiNi_{0.5}Mn_{1.5}O_{4-\delta}$ by increasing the reaction temperature from 800 °C to 900 or 1000 °C. However, the increased temperature inevitably resulted in the morphology change, which also caused the unfair comparison between the two types of materials. In fact, it is easier to form the disordered structure by adjusting the stoichiometric ratio of Ni and Mn. In this way, we can overcome the problem of morphology change during different temperatures and obtain two types of $LiNi_{0.5}Mn_{1.5}O_4$ spinel with the same morphology.

To further investigate the two types of spinel $LiNi_{0.5}Mn_{1.5}O_4$ hollow microspheres, we prepared $LiNi_{0.5-x}Mn_{1.5+x}O_4$ (x=0, 0.05, 0.1) hollow microspheres by adjusting the stoichiometric ratio of Ni and Mn. Herein, partial replacement of Ni by Mn will reduce the average valence state of Mn, introduce small amount of Mn^{3+}, and form the disordered structure. Thus, ordered $LiNi_{0.5}Mn_{1.5}O_4$, disordered $LiNi_{0.45}Mn_{1.55}O_4$, and disordered $LiNi_{0.4}Mn_{1.6}O_4$ hollow microspheres have been synthesized successfully. Furthermore, their structures and electrochemical performance have been deeply investigated.

Experimental

Spinel $LiNi_{0.5-x}Mn_{1.5+x}O_4$ (x=0, 0.05, 0.1) hollow microspheres were prepared by an impregnation method followed by a simple solid-state reaction, similar as we reported previously [13]. The $MnCO_3$ microspheres were synthesized by a precipitation method [14]. Then, the porous MnO_2 microspheres were got by decomposition of $MnCO_3$ at 400 °C for 5 h. Further, different stoichiometric $Ni(NO_3)_2\cdot 6H_2O$ and $LiOH\cdot H_2O$ were dispersed in the ethanol and impregnated in the MnO_2 microspheres to obtain a precursor after the ethanol was completely evaporated at 50 °C. Exactly, for the preparation of $LiNi_{0.5}Mn_{1.5}O_4$, 5 mmol $Ni(NO_3)_2\cdot 6H_2O$ and 10.5 mmol $LiOH\cdot H_2O$ were impregnated into 15 mmol MnO_2 microspheres. But for $LiNi_{0.45}Mn_{1.55}O_4$ and $LiNi_{0.4}Mn_{1.6}O_4$, 4.5 mmol $Ni(NO_3)_2\cdot 6H_2O$+10.5 mmol $LiOH\cdot H_2O$+15.5 mmol MnO_2 microspheres and 4 mmol $Ni(NO_3)_2\cdot 6H_2O$+10.5 mmol $LiOH\cdot H_2O$+16 mmol MnO_2 microspheres were used, respectively. Finally, the spinel hollow microspheres were obtained by calcining the precursor at 800 °C for 20 h, followed by a posttreatment at 700 °C for 10 h.

The phase structures of the spinel hollow microspheres were identified by X-ray diffraction (XRD) using a D/MAX 2500 V diffractometer in the range of 10~70° (2θ). The Fourier transform infrared spectroscopy (FTIR) analysis was performed with America Thermo Nicolet-67. The morphologies and microstructures of the spinel hollow microspheres were taken by scan electron microscope (SEM, JSM-6490LV) and high-resolution transmission electron microscope (HR-TEM, JEM-2100 F). X-ray photoelectron spectroscopy (XPS) analysis was carried out by using the America Thermo ESCALAB250 instrument.

The electrochemical performance of the spinel hollow microspheres was investigated by using CR2032 coin-type cells assembled in an argon-filled glove box (MBraun). In order to make the $LiNi_{0.5}Mn_{1.5}O_4$ electrode laminate, a slurry containing 84 wt.% active material, 8 wt.% acetylene black, and 8 wt.% polyvinylidene fluoride (PVDF) dispersed in *N*-methyl-2-pyrrolidinone (NMP) was cast onto an aluminum current collector. After vacuum drying at 70 °C, the laminate was punched into discs (Φ14 mm) as the electrode for assembling the coin cells. The mass loading in the electrode was controlled at about 6 mg cm^{-2}. Celgard 2400 microporous polypropylene membrane was used as separator. Highly pure lithium foil was used as the counter electrode and reference electrode for the cell assembly. The electrolyte was 1 M $LiPF_6$/ethylene carbonate (EC)+dimethyl carbonate (DMC) (1:1, *w*/*w*). The $Li/LiNi_{0.5}Mn_{1.5}O_4$ cells were galvanostatically cycled between 3.5 and 5 V on a multi-channel battery cycler (Neware BTS2300, Shenzhen). And all the cell tests were taken in the constant current-constant voltage (CC-CV) model. The constant voltage (CV) regime ended until the current rate was lower than 0.5 C. Electrochemical impedance spectra (EIS) measurements of the $Li/LiNi_{0.5}Mn_{1.5}O_4$ cells charged to 5.0 V were performed on a CHI 604D electrochemical workstation with applied 10 mV sinusoidal perturbation in a frequency range from 100 kHz to 10 mHz at room temperature. The EIS results were fitted by using the Z-view software.

Results and discussion

The XRD patterns of the $LiNi_{0.5-x}Mn_{1.5+x}O_4$ (x=0, 0.05, 0.1) products are shown in Fig. 1a. All the synthesized products present typical diffractions of a cubic spinel phase. With x increasing to 0.1 ($LiNi_{0.4}Mn_{1.6}O_4$), the impurity diffraction peak near (400) peak becomes obvious and it is corresponding

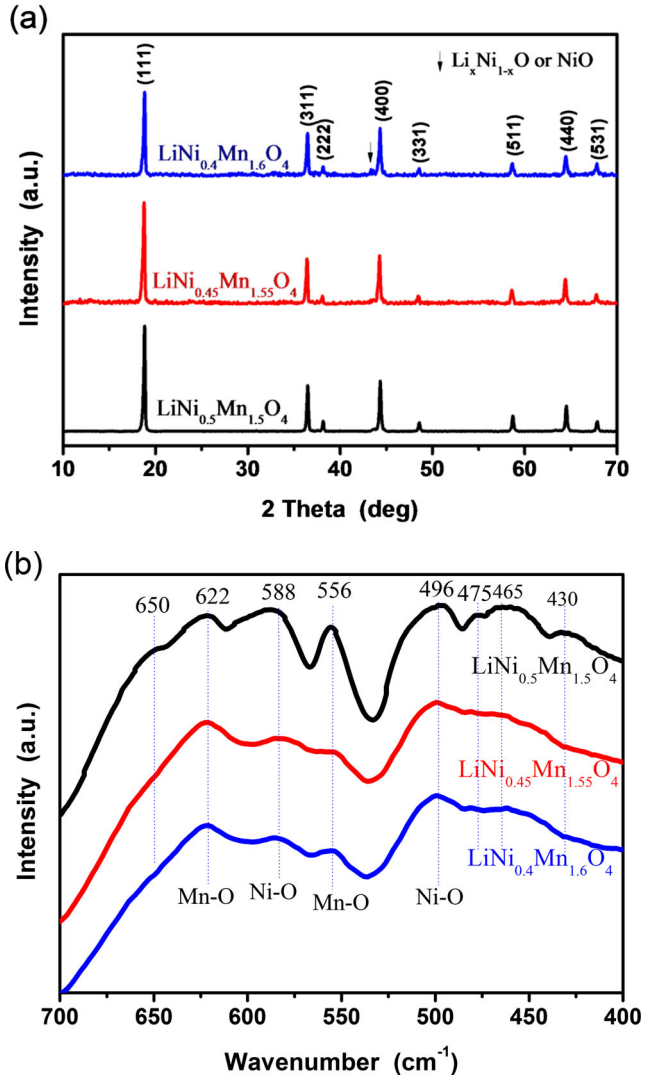

Fig. 1 XRD patterns (**a**) and FTIR images (**b**) of $LiNi_{0.5}Mn_{1.5}O_4$, $LiNi_{0.45}Mn_{1.55}O_4$, and $LiNi_{0.4}Mn_{1.6}O_4$

to $Li_xNi_{1-x}O$ or NiO_x, which was often formed in the solid-state synthesis of $LiNi_{0.5}Mn_{1.5}O_4$ [15–17]. For $LiNi_{0.5}Mn_{1.5}O_4$ and $LiNi_{0.45}Mn_{1.55}O_4$, this impurity phase is negligible. Additionally, we found that the (111) diffraction peak of $LiNi_{0.45}Mn_{1.55}O_4$ had a shift to low angle (from 18.82° to 18.75°) in $LiNi_{0.5}Mn_{1.5}O_4$. That is because partial Mn^{4+} (0.54 Å) converting to bigger Mn^{3+} (0.66 Å) by the replacement of Ni by Mn could result in the enlargement of lattice. The effect will also be confirmed by XPS below. However, in XRD, it is difficult to identify whether the sample has $P4_332$ or Fd3m structure. Thus, the FTIR spectra of the $LiNi_{0.5}Mn_{1.5}O_4$, $LiNi_{0.45}Mn_{1.55}O_4$ and $LiNi_{0.4}Mn_{1.6}O_4$ powders are investigated in Fig. 1b. Amatucci and co-workers reported that the ordered $LiNi_{0.5}Mn_{1.5}O_4$ ($P4_332$) had eight IR absorption bands while the disordered $LiNi_{0.5}Mn_{1.5}O_{4-\delta}$ (Fd3m) had only five [8, 9]. Here, $LiNi_{0.45}Mn_{1.55}O_4$ and $LiNi_{0.4}Mn_{1.6}O_4$ have five IR absorption bands at 465, 496, 556, 581, and 622 cm^{-1}, which are the fingerprint of the disordered $LiNi_{0.5}Mn_{1.5}O_{4-\delta}$ [18]. Since there are additional three peaks at 430, 478, and 650 cm^{-1}, $LiNi_{0.5}Mn_{1.5}O_4$ has low symmetry, which results from the well-separated Ni and Mn sites. Therefore, it is concluded that here, $LiNi_{0.5}Mn_{1.5}O_4$ is ordered with the space group of $P4_332$, but the other two are disordered with the space group of Fd3m.

To investigate oxidation state of Mn of $LiNi_{0.5}Mn_{1.5}O_4$, $LiNi_{0.45}Mn_{1.55}O_4$, and $LiNi_{0.4}Mn_{1.6}O_4$, XPS analysis has been carried out in Fig. 2. The sets of $Mn2p_{2/3}$ peaks in Fig. 2a–c show that Mn^{4+} and Mn^{3+} are coexistence. As shown in Fig. 2a, the majority of $LiNi_{0.5}Mn_{1.5}O_4$ product is

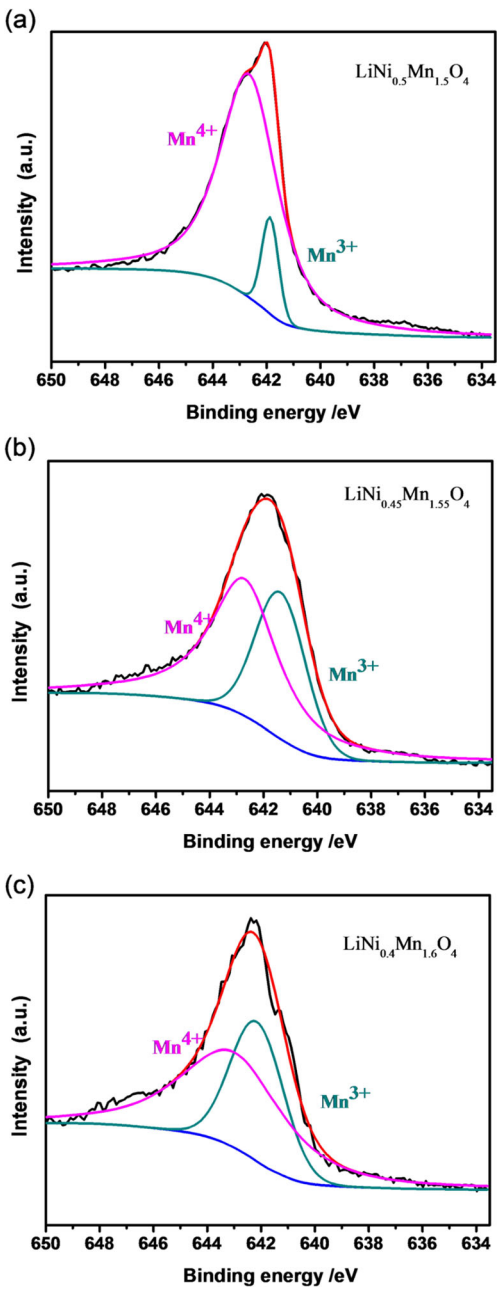

Fig. 2 Mn2p2/3 XPS spectra of $LiNi_{0.5}Mn_{1.5}O_4$ (**a**), $LiNi_{0.45}Mn_{1.55}O_4$ (**b**), and $LiNi_{0.4}Mn_{1.6}O_4$ (**c**)

mostly composed of Mn^{4+}. From a peak separation, however, in relatively low binding energy, there was a small peak, indicating that the trace amounts of Mn^{3+} exist [19, 20]. For the $LiNi_{0.45}Mn_{1.55}O_4$ and $LiNi_{0.4}Mn_{1.6}O_4$, the existence of Mn^{3+} could be found obviously. Furthermore, the amount of Mn^{3+} increased with the increment of Mn replacing Ni. As we all know, the presence of Mn^{3+} in the structure can improve the electronic and ionic conductivities [5, 7–11]. All above, from the XPS, XRD, and FTIR results, we can confirm that ordered $LiNi_{0.5}Mn_{1.5}O_4$, disordered $LiNi_{0.45}Mn_{1.55}O_4$, and disordered $LiNi_{0.4}Mn_{1.6}O_4$ samples have been synthesized successfully by adjusting the stoichiometric ratios of Ni and Mn.

Figure 3 depicts the morphologies of $LiNi_{0.5}Mn_{1.5}O_4$, $LiNi_{0.45}Mn_{1.55}O_4$, and $LiNi_{0.4}Mn_{1.6}O_4$. The low-magnification SEM images (Fig. 3a, c, e) reveal that all the products are consisted of regular microspheres with a diameter of 4~6 μm. Most $LiNi_{0.5}Mn_{1.5}O_4$ microspheres have the comparative diameter with the $LiNi_{0.45}Mn_{1.55}O_4$ microspheres, but the $LiNi_{0.4}Mn_{1.6}O_4$ microspheres are slightly smaller than the other two types of microspheres. The main reason could be the smaller amounts of Li and Ni sources impregnated into the same amount of MnO_2 microspheres during the preparation of $LiNi_{0.4}Mn_{1.6}O_4$. As shown in Fig. 3b, d, f, high-magnification SEM images illustrate that all the microspheres have the hollow structure. From Fig. 3b, the wall thickness of the hollow microspheres is about 0.5–1.0 μm. Such a thick wall can make the hollow structure keep stable during the electrode preparation. In our previous report [13], we prepared the similar hollow microspheres with different space groups under different reaction temperatures, but the different temperatures cause the obvious differences on morphology, crystallinity, and surface structure of the primary particles. But here, the primary particles for the three samples have quite similar morphology and crystallinity. Furthermore, in Fig. 4, the HR-TEM images show the single-crystalline nature of the surface for the primary particles in the three samples, and the measured neighboring interplanar distance of 0.46 nm matches well with the spacing between the (111) planes.

The initial voltage profiles of all $Li/LiNi_{0.5-x}Mn_{1.5+x}O_4$ (x= 0, 0.05, 0.1) cells are compared in Fig. 5. It is clear that all the voltage profiles at 1 C include a flat plateau at 4.7 V, corresponding to the reversible reactions of Ni^{2+}/Ni^{3+} and $Ni^{3+}/$

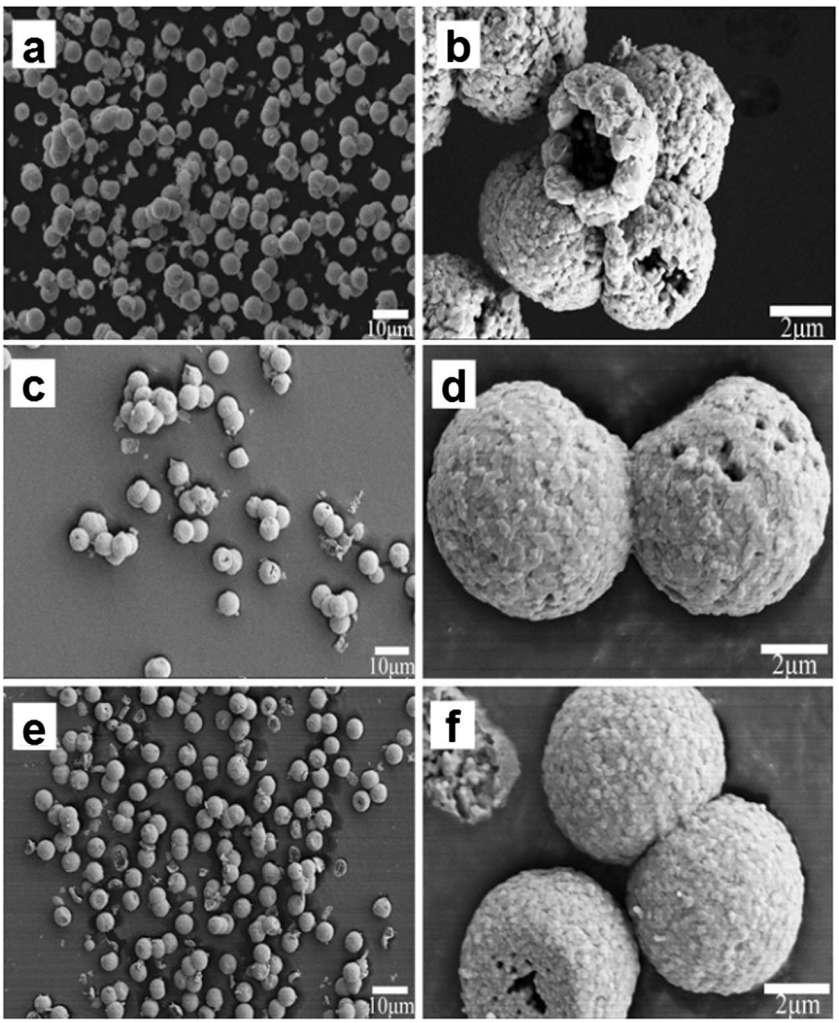

Fig. 3 SEM micrographs of $LiNi_{0.5}Mn_{1.5}O_4$ (**a**), (**b**); $LiNi_{0.45}Mn_{1.55}O_4$ (**c**), (**d**); and $LiNi_{0.4}Mn_{1.6}O_4$ (**e**), (**f**)

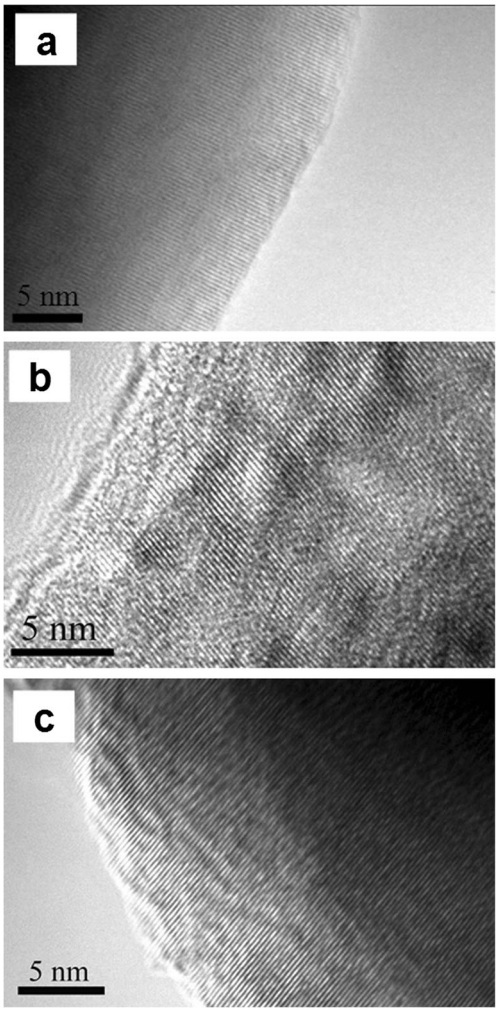

Fig. 4 HR-TEM images of $LiNi_{0.5}Mn_{1.5}O_4$ (**a**), $LiNi_{0.45}Mn_{1.55}O_4$ (**b**), and $LiNi_{0.4}Mn_{1.6}O_4$ (**c**)

Ni^{4+} [21, 22]. Furthermore, for the cells using $LiNi_{0.45}Mn_{1.55}O_4$ and $LiNi_{0.4}Mn_{1.6}O_4$, an obvious voltage plateau can be observed between 3.8 and 4.2 V, corresponding to the Mn^{3+}/Mn^{4+} redox process [23]. This also supports the fact that a small fraction of Mn^{3+} existed in disordered $LiNi_{0.45}Mn_{1.55}O_4$ and $LiNi_{0.4}Mn_{1.6}O_4$. However, the cell using the ordered $LiNi_{0.5}Mn_{1.5}O_4$ shows a negligible plateau in the 3.8~4.2 V region. The capacity of this plateau can indirectly reflect the amount of Mn^{3+} ions in the spinel materials. That is, the higher capacity results from the more Mn^{3+} ions. It is further observed that the initial discharge capacities of $LiNi_{0.5}Mn_{1.5}O_4$, $LiNi_{0.45}Mn_{1.55}O_4$, and $LiNi_{0.4}Mn_{1.6}O_4$ are 128.5, 116.5, and 115.2 mAh/g at 1 C, respectively. The lower discharge capacities of $LiNi_{0.45}Mn_{1.55}O_4$ and $LiNi_{0.4}Mn_{1.6}O_4$ can be contributed to the decrease of Ni in $LiNi_{0.5-x}Mn_{1.5+x}O_4$ and the increment of Mn^{3+}. $LiNi_{0.5}Mn_{1.5}O_4$ and $LiNi_{0.45}Mn_{1.55}O_4$ have the comparable coulombic efficiencies of 88.7 and 90.3 %, respectively, but $LiNi_{0.4}Mn_{1.6}O_4$ has the lower coulombic efficiency of 80.6 %, probably because of the existence of $Li_xNi_{1-x}O$ impurities [24, 25].

Rate capabilities of all $Li/LiNi_{0.5-x}Mn_{1.5+x}O_4$ (x=0, 0.05, 0.1) cells are presented in Fig. 6. At 1 C and 2 C, $LiNi_{0.5}Mn_{1.5}O_4$ exhibits much higher discharge capacities than $LiNi_{0.45}Mn_{1.55}O_4$ and $LiNi_{0.4}Mn_{1.6}O_4$. However, at 5 C, $LiNi_{0.45}Mn_{1.55}O_4$ has the comparative capacity with $LiNi_{0.5}Mn_{1.5}O_4$, even though the capacity of $LiNi_{0.4}Mn_{1.6}O_4$ has a large fading. At 10 C, the disordered $LiNi_{0.45}Mn_{1.55}O_4$ can deliver the higher discharge capacities of 96.8 mAh/g than the ordered $LiNi_{0.5}Mn_{1.5}O_4$ (85 mAh/g). Among the three samples, $LiNi_{0.4}Mn_{1.6}O_4$ presents the lowest discharge capacities at various rates, which is mainly attributed to the presence of $Li_xNi_{1-x}O$ impurities [25]. In our previous work, the ordered $LiNi_{0.5}Mn_{1.5}O_4$ hollow microspheres were synthesized with superior rate capability and good cycling stability, which were much better than the disordered $LiNi_{0.5}Mn_{1.5}O_4$ [13]. But in this work, we prepare the spinel $LiNi_{0.5-x}Mn_{1.5+x}O_4$ (x=0, 0.05, 0.1) hollow microspheres with quite similar structure and find that the disordered $LiNi_{0.45}Mn_{1.55}O_4$ exhibits better rate capability than the ordered $LiNi_{0.5}Mn_{1.5}O_4$ at high rates. As reported previously, disordered (Fd3m) $LiNi_{0.5}Mn_{1.5}O_5$ presented large diffusion coefficient of Li^+ (D_{Li}^+) than the ordered ($P4_332$) in grain because of the existence of Mn^{3+} with the higher ionic conductivity and the large ionic radius in disordered $LiNi_{0.5}Mn_{1.5}O_4$ [7–9]. In addition, as recently reported [26–28], single-crystal nanostructures

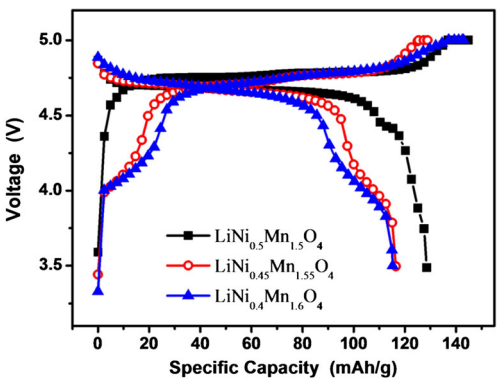

Fig. 5 Initial charge/discharge curves of $LiNi_{0.5}Mn_{1.5}O_4$, $LiNi_{0.45}Mn_{1.55}O_4$, and $LiNi_{0.4}Mn_{1.6}O_4$

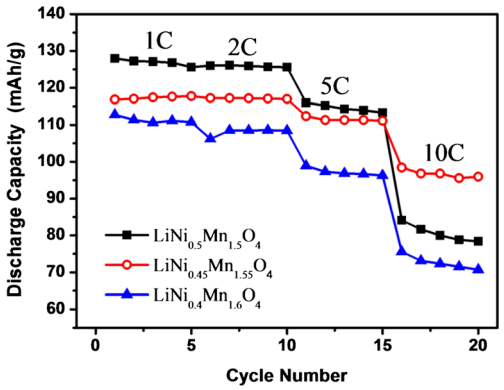

Fig. 6 Rate performance of $LiNi_{0.5}Mn_{1.5}O_4$, $LiNi_{0.45}Mn_{1.55}O_4$, and $LiNi_{0.4}Mn_{1.6}O_4$

favor charge transfer and accelerate the electrochemical reactions. Therefore, we believe that the higher rate capability of $LiNi_{0.45}Mn_{1.55}O_4$ is attributed to both the high ionic conductivity and the large ionic transfer channel of the existed Mn^{3+} and the single-crystal surface configuration that also benefits for Li insertion and extraction [7–9, 13].

Cycling performance of $Li/LiNi_{0.5-x}Mn_{1.5+x}O_4$ (x=0, 0.05, 0.1) cells is shown in Fig. 7, and all the three samples exhibit quite good cycling stability, possibly because of the unique nano/micro hierarchical structure. Also, their good cycling performance suggests that the hollow structure is stable enough during cycling. To understand the electrochemical performance in depth, EIS was carried out by using $Li/LiNi_{0.5-x}Mn_{1.5+x}O_4$ (x=0, 0.05, 0.1) cells after the third cycle, shown in Fig. 8. All impedance spectra show a similar profile consisting of two semicircles and a sloping line. The semicircle in the high-to-medium frequency range is ascribed to the process of Li^+-ion migration through the surface layer, the other semicircle in the medium-to-low frequency range is related to the charge transfer kinetics of the electrode, and the sloping line in the low frequency range is for the diffusion of Li^+ in the solid electrode [29–33]. The impedance spectra can be explained on the basis of an equivalent circuit (inset of Fig. 8), and the fitting results are summarized in Table 1. In the equivalent circuit, Re represents the electrolyte resistance, Rs is the surface impedance, and Rct is the charge transfer impedance. CPE1 and CPE2 signify the corresponding constant-phase elements, which describe the nonideal capacitances of the surface layer and the double layer, respectively. Zw is the Warburg impedance. From Table 1, there is only negligible difference on Re, but remarkable difference can be found on Rs and Rct between the three samples. $LiNi_{0.5}Mn_{1.5}O_4$ has the lower Rs of 19.4 Ω than $LiNi_{0.45}Mn_{1.55}O_4$ (25.2 Ω) and $LiNi_{0.4}Mn_{1.6}O_4$ (46.2 Ω), explaining for the higher initial capacity of $LiNi_{0.5}Mn_{1.5}O_4$ at low rates (1 C and 2 C). But the Rct (26.4 Ω) of $LiNi_{0.5}Mn_{1.5}O_4$ is higher than that of $LiNi_{0.45}Mn_{1.55}O_4$ (19.0 Ω). Since the lower Rct is highly significant for the superior

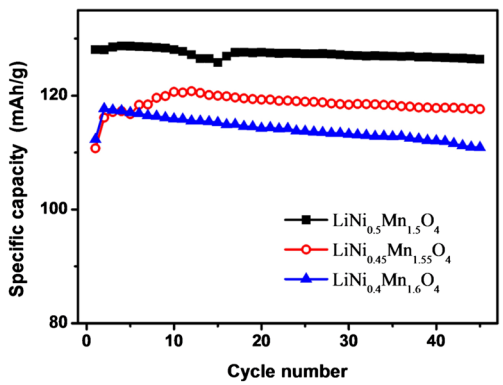

Fig. 7 Cycling performance of $LiNi_{0.5}Mn_{1.5}O_4$, $LiNi_{0.45}Mn_{1.55}O_4$, and $LiNi_{0.4}Mn_{1.6}O_4$

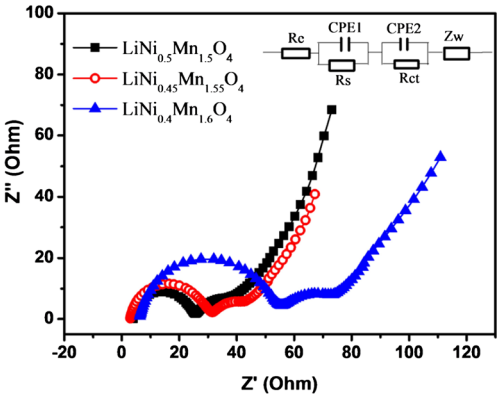

Fig. 8 EIS spectra of $LiNi_{0.5}Mn_{1.5}O_4$, $LiNi_{0.45}Mn_{1.55}O_4$, and $LiNi_{0.4}Mn_{1.6}O_4$ after 3 cycles. The *insert* represents equivalent circuit

rate capability, $LiNi_{0.45}Mn_{1.55}O_4$ exhibits the better rate capability than $LiNi_{0.5}Mn_{1.5}O_4$ and $LiNi_{0.4}Mn_{1.6}O_4$ at high rates. Basically, the good charge transfer kinetics of $LiNi_{0.45}Mn_{1.55}O_4$ is attributed to the increased electronic conductivity and Li^+ diffusion ability from the participation of Mn^{3+}, even though too many Mn^{3+} in $LiNi_{0.4}Mn_{1.6}O_4$ could increase both Rs and Rct as the result of the distortion of the lattice and the undesirable disproportionation. Therefore, introducing a moderate amount of Mn^{3+} in $LiNi_{0.5}Mn_{1.5}O_4$ with the Fd3m, space group significantly improves the rate capability of the spinel hollow microspheres.

Conclusions

In summary, the ordered and disordered spinel hollow microspheres with highly similar structure were synthesized by simply adjusting the stoichiometric ratio of Ni/Mn in $LiNi_{0.5-x}Mn_{1.5+x}O_4$ (x=0, 0.05, 0.1). $LiNi_{0.5}Mn_{1.5}O_4$ is the ordered, but $LiNi_{0.45}Mn_{1.55}O_4$ and $LiNi_{0.4}Mn_{1.6}O_4$ are the disordered along with the presence of Mn^{3+} in the lattice. Although the ordered $LiNi_{0.5}Mn_{1.5}O_4$ hollow microspheres deliver the highest capacity at low rates among the three spinel materials, the disordered $LiNi_{0.45}Mn_{1.55}O_4$ hollow microspheres exhibit the superior rate capability at high rates. That is, the disordered spinel $LiNi_{0.5-x}Mn_{1.5+x}O_4$ with a moderate amount of Mn^{3+} has the better electrochemical performance than the ordered spinel with the similar morphology and structure. The improved high rate capability of $LiNi_{0.45}Mn_{1.55}O_5$ is attributed to the combination of the increased electronic conductivity

Table 1 Impendence parameters calculated from equivalent circuit

	R_e (Ω)	R_s (Ω)	R_{ct} (Ω)
$LiNi_{0.5}Mn_{1.5}O_4$	4.0	19.4	26.4
$LiNi_{0.45}Mn_{1.55}O_4$	3.2	25.2	19.0
$LiNi_{0.4}Mn_{1.6}O_4$	6.2	46.2	22.3

and Li^+-ion diffusion by moderate Mn^{3+} incorporation, along with the hierarchical structure. Therefore, adjusting good stoichiometric ratio of Ni and Mn in $LiNi_{0.5-x}Mn_{1.5+x}O_4$ is proved as an efficient way to improve the electrochemical performance of $LiNi_{0.5}Mn_{1.5}O_4$ spinel hollow microspheres. The obtained $LiNi_{0.45}Mn_{1.55}O_4$ hollow microspheres are worthy of further investigation and application as cathode material for advanced Li-ion batteries.

Acknowledgments This study was supported by National Science Foundation of China (Grant Nos. 21006033 and 51372060) and the Fundamental Research Funds for the Central Universities (2013HGCH0002).

References

1. Armand M, Tarascon JM (2008) Nature 451:652
2. Bruce PG, Scrosati B, Tarascon JM (2008) Angew Chem Int Ed 47: 2930
3. Zhong GB, Wang YY, Zhang ZC, Chen CH (2011) Electrochim Acta 56:6554
4. Yi TF, Xie Y, Ye MF, Jiang LJ, Zhu RS, Zhu YR (2011) Ionics 17:383
5. Kim JH, Myung ST, Yoon CS, Kang SG, Sun YK (2004) Chem Mater 16:906
6. Amdouni N, Zaghib K, Gendron F, Mauger A, Julien CM (2006) Ionics 12:117
7. Kunduraci M, Amatucci GG (2008) Electrochim Acta 53:4193
8. Kunduraci M, Al-Sharab J, Amatucci G (2006) Chem Mater 18:3585
9. Kunduraci M, Amatucci GG (2006) J Electrochem Soc 153:A1345
10. Shaju KM, Bruce PG (2008) Dalt Trans 40:5471
11. Wang LP, Li H, Huang XJ, Baudrin E (2011) Solid State Ionics 193: 32
12. Ma XH, Kang B, Ceder G (2010) J Electrochem Soc 157:A925
13. Wu WW, Xiang HF, Zhong GB, Su W, Tang W, Zhang Y, Yu Y, Chen CH (2014) Electrochim Acta 119:206
14. Fei JB, Cui Y, Yan XH, Qi W, Yang Y, Wang KW, He Q, Li JB (2008) Adv Mater 20:452
15. Huang H, Chen CH, Perego RC, Kelder EM, Chen L, Schoonman J, Weydanz WJ, Nielsen DW (2000) Solid State Ionics 127:31
16. Zhou L, Zhao DY, Lou XW (2012) Angew Chem Int Ed 51:239
17. Liu YJ, Chen L (2012) Ionics 18:649
18. Song J, Shin DW, Yu Y, Amos CD, Manthiram A, Goodenough JB (2012) Chem Mater 24:3101
19. Yang TY, Zhang NQ, Lang Y, Sun KN (2011) Electrochim Acta 56: 4058
20. Hao XG, Austin MH, Bartlett BM (2012) Dalt Trans 41:8067
21. Ariyoshi K, Iwakoshi Y, Nakayama N, Ohzuku T (2004) J Electrochem Soc 151:A296
22. Xu HY, Xie S, Ding N, Liu BL, Shang Y, Chen CH (2006) Electrochim Acta 51:4352
23. Ohzuku T, Takeda S, Iwanaga M (1999) J Power Sources 81:90
24. Kawaura H, Takamatsu D, Mor Si, Orikasa Y, Sugaya H, Murayama H, Nakanishi K, Tanida H, Koyama Y, Arai H, Uchimoto Y, Ogumi Z (2014) J Power Sources 245:816.
25. Zhang XF, Liu J, Yu HY, Yang GL, Wang JW, Yu ZJ, Xie HM, Wang RS (2010) Electrochim Acta 55:2414
26. Zhang GQ, Wu HB, Hoster HE, Chan-Park MB, Lou XW (2012) Energy Environ Sci 5:9453
27. Lu ZY, Rui XH, Tan HT, Zhang WY, Hng HH, Yan QY (2013) Chempluschem 78:218
28. Lee S, Cho Y, Song H-K, Lee KT, Cho J (2012) Angew Chem Int Ed 51:8748
29. Liu J, Manthiram A (2009) Chem Mater 21:1695
30. Liu J, Manthiram A (2009) J Electrochem Soc 156:A833
31. Zhang NQ, Yang TY, Lang Y, Sun KN (2011) J Alloys Compd 509: 3783
32. Wu HM, Belharouak I, Abouimrane A, Sun YK, Amine K (2010) J Power Sources 195:2909
33. Mao J, Dai KH, Zhai YC (2012) Electrochim Acta 63:381